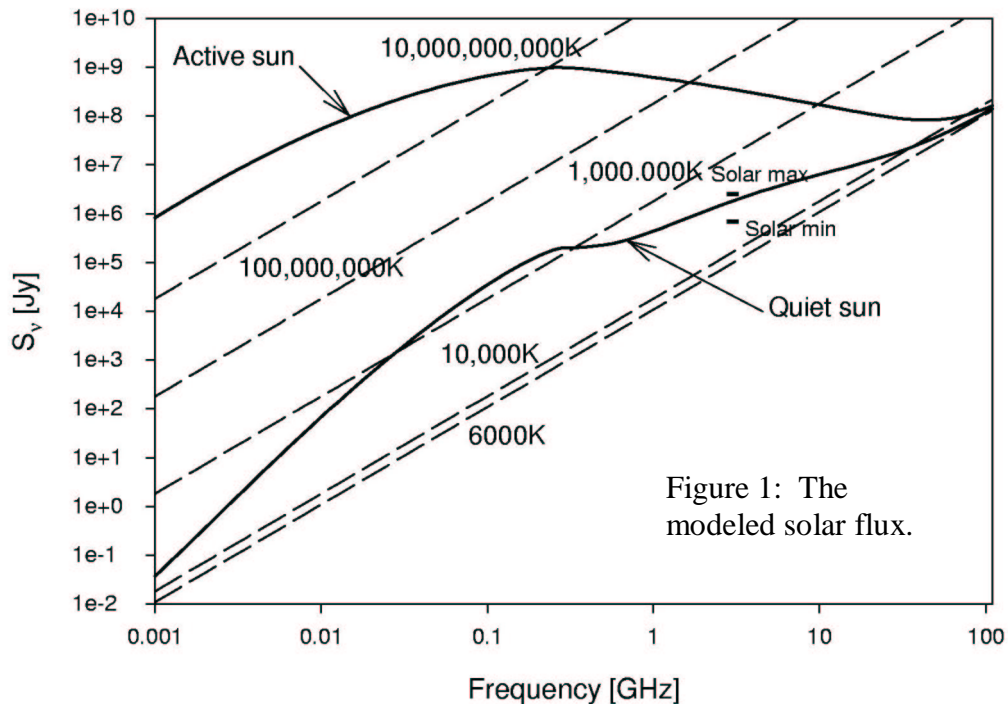


# Effects of the Sun and RFI on the ATA Offset Gregorian Antenna

David DeBoer and Geoff Bower  
February 13, 2001

## Abstract

During episodes of high sunspot activity, the sun becomes extremely bright at long wavelengths. This memo will quantify that effect and investigate the total bandwidth dependence. In addition, the primary sources of satellite radio frequency interference (RFI) will be investigated and quantified with regard to the power available at the LNA. The ATA offset Gregorian antenna to which this analysis is applied is discussed in ATA Memo 16.



## The Sun

Figure 1 shows the modeled solar flux for an “active” and “quiet” sun, along with some blackbody radiation curves and a pair of measured data points taken from the 50-year record at DRAO ([www.ngdc.noaa.gov/stp/stp.html](http://www.ngdc.noaa.gov/stp/stp.html)). At frequencies greater than about 15 GHz, the sun is reasonably well modeled by a 6000 K blackbody, while below it varies dramatically, peaking at about 300 MHz. The integrated flux is given by

$$S = \int_{\nu_1}^{\nu_2} S_\nu d\nu \quad \text{W/m}^2$$

while the available power is given by

$$W = \int_{\nu_1}^{\nu_2} A_e \iint_{src} S_\nu(\Omega) P(\Omega) d\Omega d\nu \quad W$$

where  $A_e$  is the effective area of the antenna and  $P(\Omega)$  is the normalized beam pattern such that  $P(\text{boresight})=1$ . For a uniform disc source on order of or less than the size of the antenna half-power beamwidth and a Gaussian beam, the measured power may then be expressed as

$$W = \int_{\nu_1}^{\nu_2} A_e \varepsilon(\nu) S_\nu d\nu \quad W$$

where

$$\varepsilon(\nu) \approx \frac{(1 - e^{-0.23 X \xi_s^2})}{0.23 X \xi_s^2}$$

with

$$\xi_s = \theta_s / \theta_{X\text{dB}}$$

$\theta_s$  is the source diameter

$\theta_{X\text{dB}}$  is the  $X^{\text{th}}$  dB beamwidth (e.g.  $X=3$  dB).

For the sun,  $\theta_s=0.5^\circ$  and for the ATA,  $\theta_{3\text{dB}} \approx 3.5/\nu^\circ$ , with frequency given in GHz. Figure 2 plots this correction factor. The effective area has also been estimated for a low-frequency focus setting and a high-frequency focus setting and the resulting efficiencies are also shown in Figure 2. These are the values used in the boresight pointing integrated main beam available power shown in the figures below.

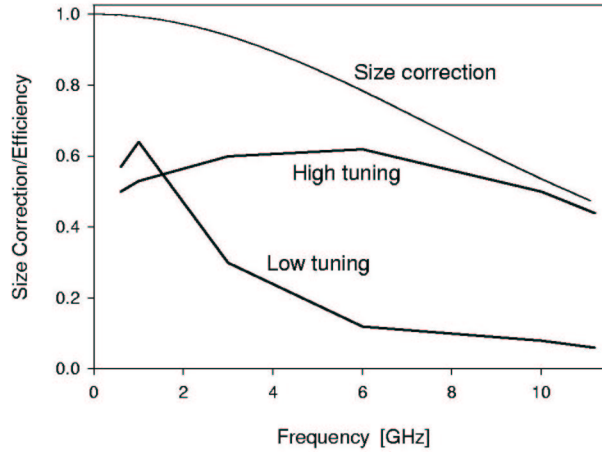


Figure 2: Size correction factor to convert flux/beam to flux for the sun and moon and efficiency models.

Figure 3 plots  $S$ ,  $W$ ,  $W_{0\text{dBi}}$  and the system power with respect to the lower frequency bound in the integration,  $\nu_1$ .  $S$  and  $W$  are given as above and  $\nu_2=11.2$  GHz.  $W_{0\text{dBi}}$  is the power into a 0dBi sidelobe, so  $A_e=\lambda^2/4\pi$  and  $\varepsilon$  is assumed to be 1. Therefore

$$W_{0\text{dBi}}(\nu_1) = 7.16 \times 10^{-3} \int_{\nu_1}^{11.2} S_\nu / \nu^2 d\nu \quad W.$$

The system power is  $k_B T_{\text{sys}} B$  where  $k_B=1.38 \times 10^{-23}$  J/K is Boltzmann's constant,  $T_{\text{sys}}$  is assumed to be 40 K and  $B=\nu_2-\nu_1$  is the bandwidth. Figure 4 shows the same plot for the quiet sun. Also included in Figures 3 and 4 are powers from some satellites, as discussed below.

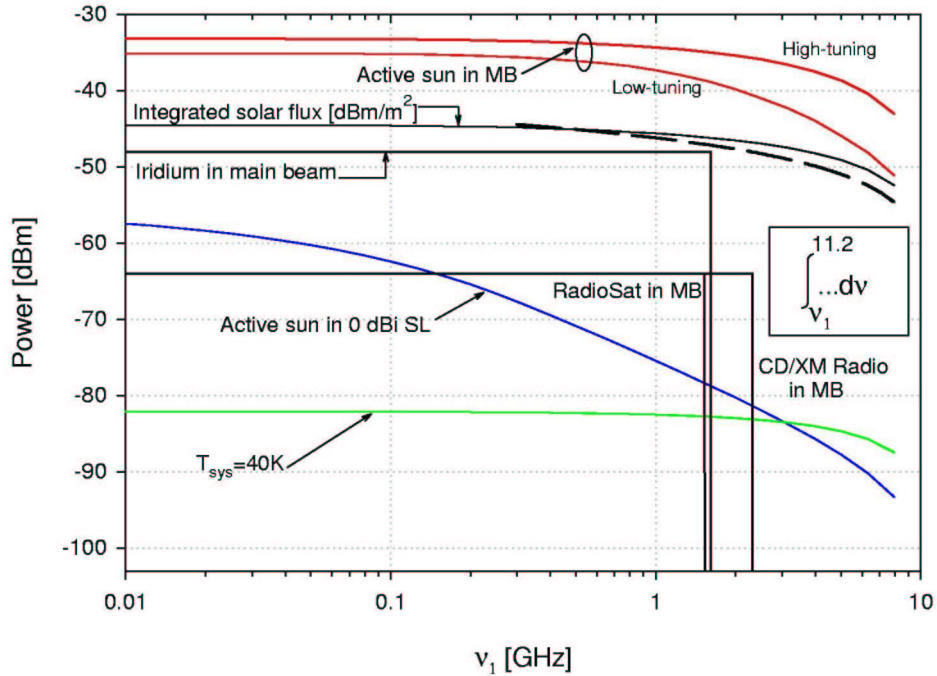


Figure 3: Integrated flux of the active sun, along with Iridium and satellite radio (RadioSat, XM Radio and CD Radio).

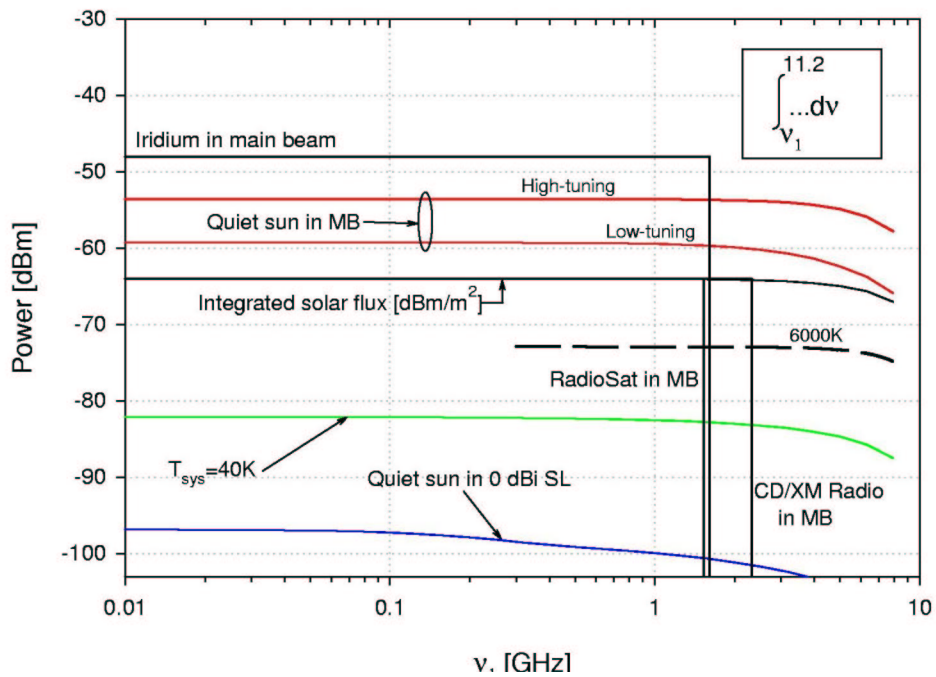


Figure 4: Integrated flux of the quiet sun, along with Iridium and satellite radio (RadioSat, XM Radio and CD Radio). Note that the integrated solar flux is coincident with the satellite radio power.

To verify these solar calculations, some back-of-the-envelope estimates may be performed. To first order over the frequency range of interest (from about 0.3-11 GHz), the maximum solar flux may be approximated as

$$S_v = 10^9(v/10^9 \text{ Hz})^{-1} \text{ Jy}$$

so the integrated flux is then

$$S = 10^{-5} \ln(v_2/v_1) \text{ mW/m}^2.$$

This expression is included as the dashed line in Figure 3. As an (unrealistic) lower limit, the sun may be viewed as a 6000 K source, such that

$$S_v = 1.1 \times 10^4 (v/10^9 \text{ Hz})^2 \text{ Jy}$$

so that

$$S = 3.67 \times 10^{-11} [(v_2/10^9)^3 - (v_1/10^9)^3] \text{ mW/m}^2$$

which is included as the dashed line in Figure 4.

The sun exhibits a great deal of variability and the active sun modeled above is essentially an upper envelope of flux from the sun. In order to adequately characterize the effects of the active sun on the ATA, one needs an estimate of the solar flux as a function of time and frequency. On the basis of a literature search and discussions with solar radio astronomers, this probability distribution is not readily available. The following is an attempt to gain order of magnitude estimates of the probability function,  $P(S > S_0)$ . For more information, refer to e.g. Kundu (1965).

Fluctuations of flux density from the sun are typically divided by wavelength into three categories: centimeter, decimeter and meter wavelength bursts. Each of these contain multiple sub-categories, with widely different behaviors. All flux density units are in terms of solar flux units ( $1 \text{ sfu} = 10^4 \text{ Jy}$ ). Broadly speaking, maximum fluxes are on the order of  $10^4 \text{ sfu}$  at cm wavelengths and  $10^5 \text{ sfu}$  at dm and m wavelengths. The mean solar flux is on the order of 100 sfu over this range.

Centimeter wavelength bursts occur with a frequency

$$f = \frac{dN}{\log dS dt} = 10^{-3} S^{-1.5} \text{ sec}^{-1}.$$

This is the number of bursts per unit time per log flux density interval, which is based on two years of observation at 3 and 10.7 cm shortly following solar maximum. The observed bursts during this time period were in the range of 1000 sfu. There are examples of bursts with  $S = 10^4 \text{ sfu}$ , but these appear to be rare.

Duration of bursts is also a function of flux density. This distribution is bivariate, with short duration bright bursts and long duration fainter bursts. The high flux density burst length may be modeled as

$$\Delta T = 100 S^{0.5} \text{ sec}$$

and the lower flux density branch as

$$\Delta T = 100 S^2 \text{ sec},$$

with a maximum of  $10^4 \text{ sec}$ . Thus, the differential probability distribution for high flux density flares is

$$P \log dS = \frac{dN}{\log dS dt} \Delta T \log dS = 0.1 S^{-1}.$$

This is an estimate of the fractional time that a flare will attain a given value. Thus the probability of  $S \sim 10^3$  sfu is  $10^{-4}$ , which amounts to  $<10$  1000sec events during the year. Bursts at  $S \sim 10$  sfu occur daily. Figure 5 plots the expressions for  $f$ ,  $\Delta T$  and  $P \log dS$ . This value gets added to the mean solar flux of about  $10^6$  Jy so only the values with flux  $>10^6$  Jy will contribute appreciably to the overall measured flux. You will note that the plotted active sun in Figure 1 will occur only about 0.0004% of the time, but likely skewed towards solar maximum. The active sun in Figure 1 could then be thought of as the 99.9996%ile sun. The 95%ile sun is essentially the quiet sun, at least at centimeter wavelengths.

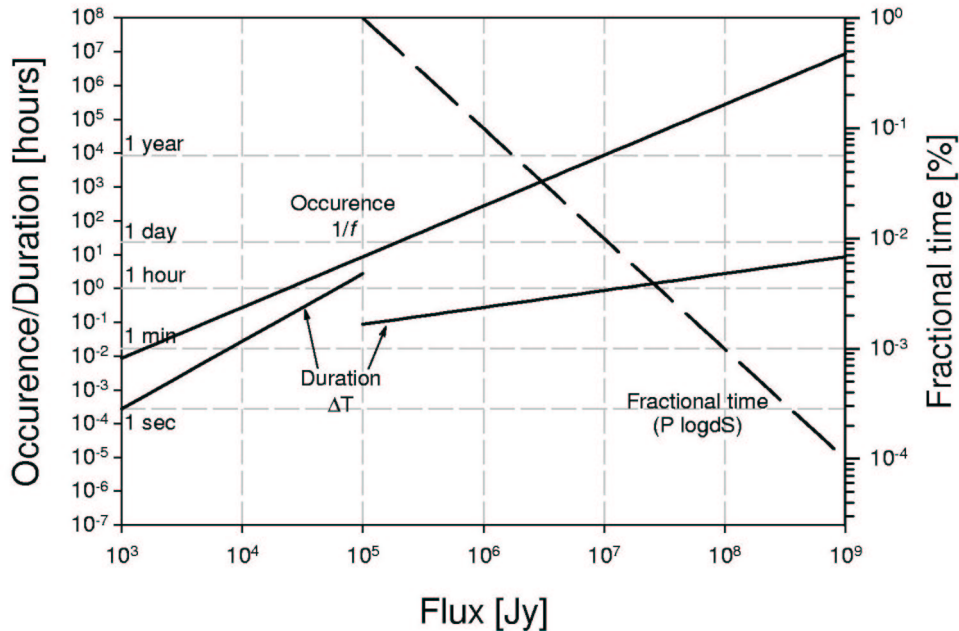


Figure 5: Properties of the centimeter-wavelength bursts. This flux is superposed over the mean solar value of about  $10^6$  Jy.

Decimeter bursts tend to be correlated with centimeter wavelength bursts. They have similar maxima and are usually longer in duration. They may also include features with narrow frequency characteristics and very short ( $<1$  s) durations. These are often correlated with meter wavelength bursts.

Meter wavelength bursts occur more frequently and have higher flux densities than centimeter or decimeter wavelength bursts. However, they are typically narrow band ( $\sim <300$  MHz) events so that they will not dominate the total noise power. These events have been observed to frequencies as low as 10 MHz. Maximum flux densities are on the order  $10^5$  sfu but are typically  $10^2$  sfu. Type III bursts are the most common. During solar maximum, these short duration (a few sec) bursts will occur several times per hour. Type II bursts, which are a few minutes in duration, occur  $\sim < 1$ /day.

## Radio Frequency Interference (RFI)

RFI from orbiting satellites will also affect the operating environment of the electronics at each antenna. Table I lists some of the expected power levels available at the LNA for different satellites, where the “high-frequency” focusing for the feed has been used in the relevant quantities. You will note that Iridium into a +2 dBi sidelobe roughly doubles the system noise power, as does GPS in the main beam. Iridium as viewed at boresight has also been plotted into the main beam in Figures 3 and 4, as are the satellite radio signals. To scale these for different sidelobe levels, just move the curve down the appropriate number of dB.

**Table I**

		<b>GPS</b>	<b>Iridium</b>	<b>Satellite radio</b>	<b>Radarsat</b>
<b>Power density (dBm/m<sup>2</sup>)</b>		-95	-60	-76	0
<b>MB</b>	<b>Power available at LNA (dBm)</b>	-83	-48	-64	+12
	<b>Dynamic range (dB)</b>	2.5	34	18	!!!
	<b>Source equivalent in 11 GHz band</b>	2.9 kJy 140 Hyd A	9MJy 3.5 Quiet Suns	230 kJy 212 Cas A	9 TJy 39k Active Suns
<b>10dBi</b>	<b>Power available at LNA (dBm)</b>	-110	-75	-91	-26
	<b>Source equivalent in 11 GHz band</b>	5 Jy	16 kJy 15 Cas A	455 Jy 5 Vir A	13 MJy 6 Active Suns

The Iridium power is dominated by a narrow-band ringer tone, with the actual “signal” being relatively insignificant. This tone is not always present, but is there frequently enough to need to be accounted for. The full Iridium band is 1610-1627 MHz. Iridium is in a circular orbit at an altitude of 780 km and doesn’t appear to be going away soon. GPS is in an orbit at about 20,200 km (halfway to geostationary orbit) and the quoted figure assumes the satellite is overhead. Note that many GPS satellites will be visible at one time, so the aggregate GPS contribution into the sidelobes could well be >8 dB greater into the mean sidelobe level. It should still have negligible impact on the system performance, however. The proposed L5 band on Block III will likely be about 5 dB stronger than L1.

There are three satellite radio systems: RadioSat, CD Radio and XM Radio. These all originate from geostationary satellites with an EIRP of about 57 dBW at Hat Creek. RadioSat rents L-band transponders from the Canadian satellite MSAT at 106.5° W, CD Radio will eventually have three satellites (80° W, 110° W and TBD), and XM Radio will shortly have two satellites (*Rock and Roll*). CD Radio (*aka* Sirius) and XM Radio are both S-band systems operating at 2320-2332 MHz. They represent the strongest geostationary signal we are likely to see.

Radarsat is obviously a potential threat and the exact EIRP is difficult to ascertain. The antenna is a 15m×1.5M antenna and the average transmitter power is 300W, but the peak is 5 kW. It operates at 5.3 GHz in a 30 MHz bandwidth. It's sun-synchronous orbit is at an altitude of about 800 km, which yields a potential EIRP of about 100 dBW, or 0 dBm/m<sup>2</sup> on the ground. This is +12dBm at the LNA, which would potentially physically damage the LNA. This may be an alarmist scenario, but the presence of Radarsat (and any potential Shuttle or ISS imaging radars) must certainly be noted.

## Conclusions

The sun as seen by the ATA offset Gregorian antenna has been analyzed, both in terms of levels and frequency. The most likely sun is the "quiet" sun and will pose no obstacle to observing, provided it stays out of the main beam. The quiet sun may even be observed with a modest amount of attenuation after the LNA. The active sun will affect operations, as it will swamp the system temperature even when in a distant side-lobe. Fortunately this occurs less than about 0.1% of the time. There is no placement of a high-pass filter edge that will mitigate the active sun anywhere in the beam.

Barring a catastrophic observation of an orbiting radar imager, Iridium is the biggest source of satellite rfi in the sky. Iridium in a +2 dBi sidelobe will present the equivalent of the system noise temperature to the LNA. When operating in the nominal high-pass focus setting, this is about 5% of the sky clustered near the main lobe. When in focus this drops to about 1%. The satellite radio signals (RadioSat, CD/XM Radio) must pass within the main lobe to double the system temperature.

The geostationary arc is well-populated and represents an arc of declination at about 6°S that must largely be avoided, although there are fortunately no satellites over the Pacific Ocean. Figure 6 shows a calculation of the power available at the LNA for an antenna similar to the ATA offset Gregorian (same 3dB beamwidth, however the beam pattern is a scaled  $J_1(x)/x$  Airy disc with approximate "high-tuning" efficiencies; see Memo 16) with an estimate of the flux available from satellites based on literature found on the Internet. The Hat Creek Radio Observatory is the assumed ground position (121°28'14"W, 40°49'02" N, 1021 m). The gap over the Pacific Ocean is clearly visible, as are the two strong L-band satellites, MSAT-1 and AMSC-1. Figure 7 includes an Iridium satellite at an arbitrary location using the flux measured as part of the RFI investigation carried out in preliminary site analyses; as well as a GPS satellite, with assumed flux based on published data. The color scale represents power available to the LNA in dBm. Note that the dark blue represents the system noise power (about -82 dBm).

## Reference

Kundu, M.R. 1965, Solar Radio Astronomy, John Wiley & Sons, New York

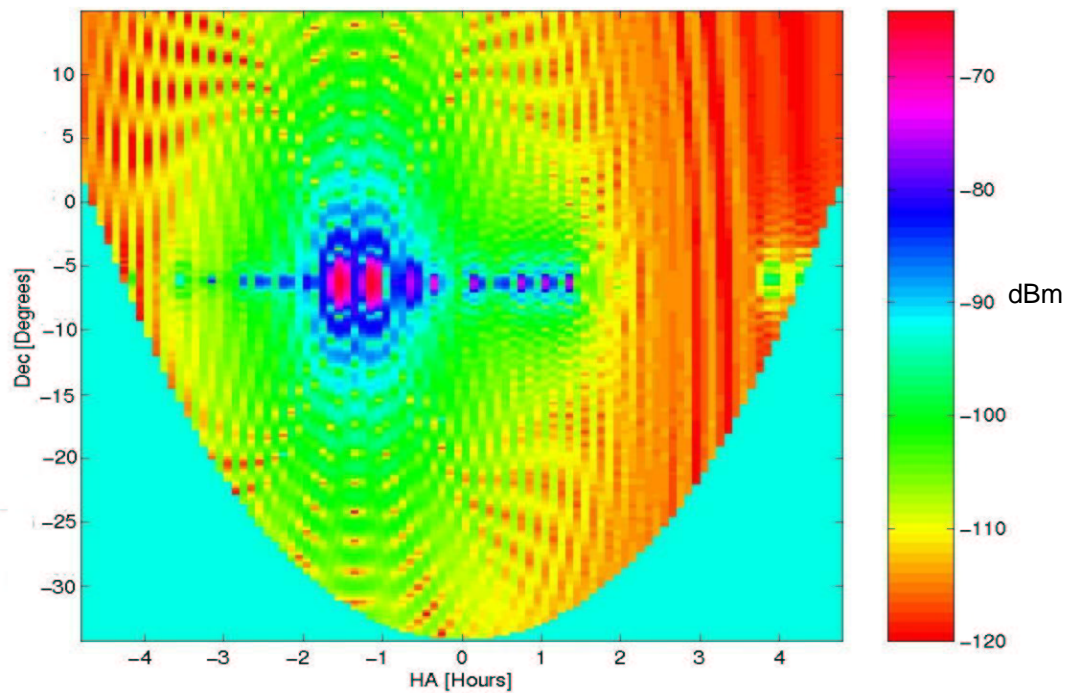


Figure 6: Geostationary arc, as seen from HCRO using an antenna similar to the ATA offset Gregorian. The scale is dBm available to the LNA. The  $15^\circ$  horizon is blanked. (Note that red wraps around the color bar.)

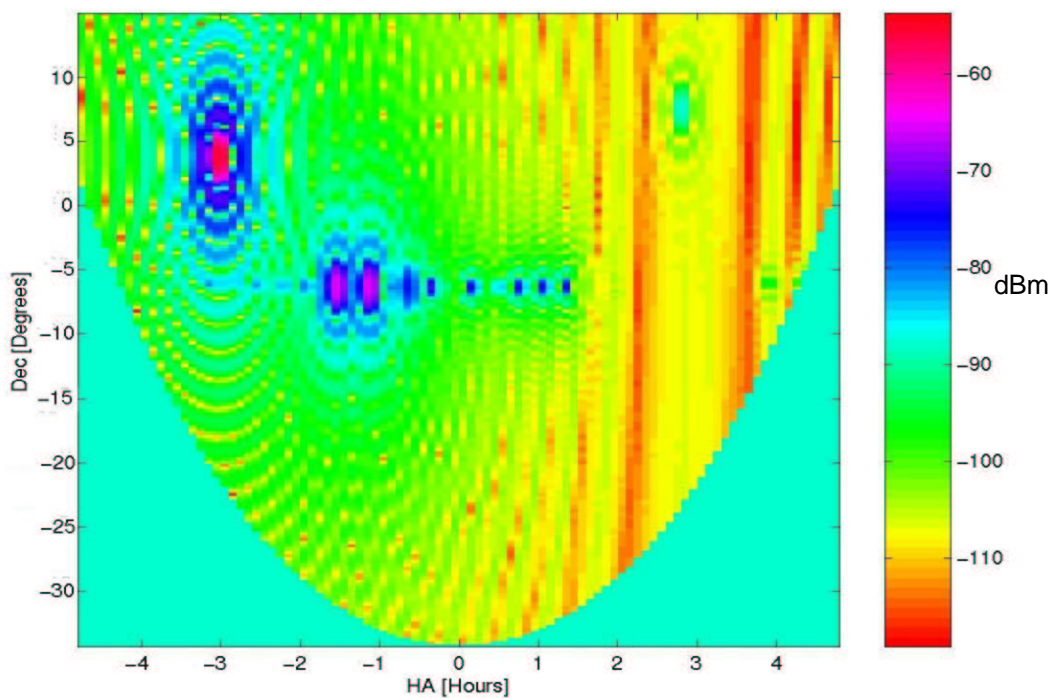


Figure 7: Similar plot to Figure 6, with the inclusion of Iridium and GPS. Iridium is very obvious. GPS is the light blue spot at about HA=3, Dec=7.